Reduction kinetics analysis of sol–gel-derived $CuO/CuAl_2O_4$ oxygen carrier for chemical looping with oxygen uncoupling

Lei Guo, Haibo Zhao, Kun Wang, Daofeng Mei, Zhaojun Ma & Chuguang Zheng

Journal of Thermal Analysis and Calorimetry
An International Forum for Thermal Studies

ISSN 1388-6150
Volume 123
Number 1

J Therm Anal Calorim (2016)
123:745-756
DOI 10.1007/s10973-015-4904-6

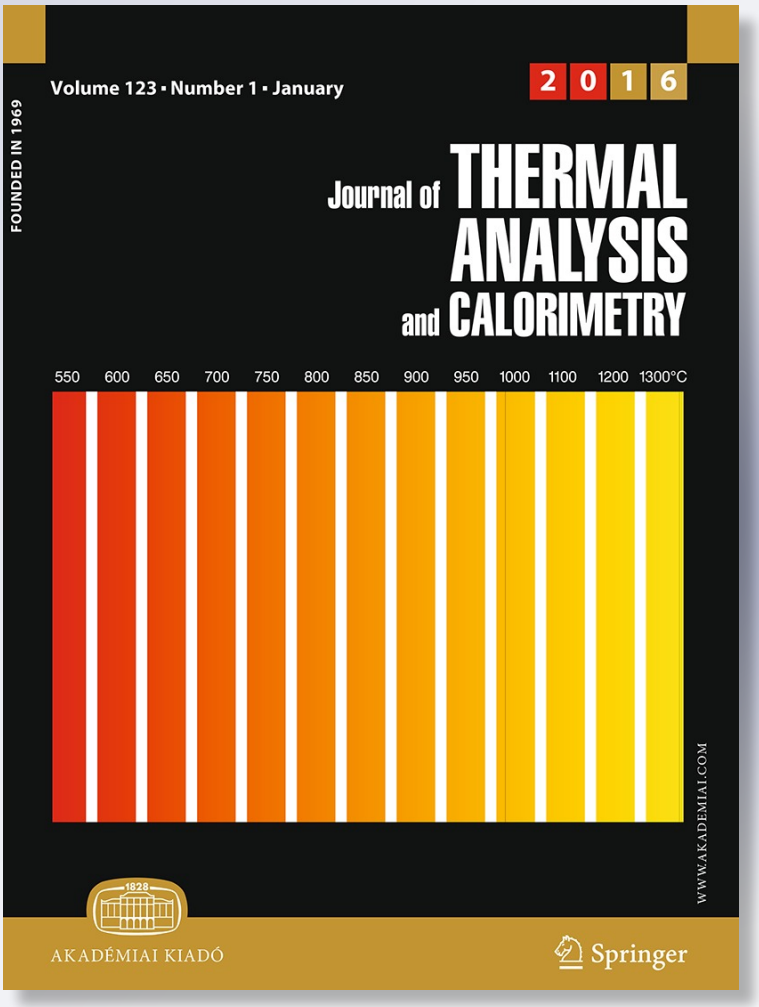

Springer

J Therm Anal Calorim (2016) 123:745–756
DOI 10.1007/s10973-015-4904-6

Reduction kinetics analysis of sol–gel-derived $CuO/CuAl_2O_4$ oxygen carrier for chemical looping with oxygen uncoupling

Lei Guo[1] · Haibo Zhao[1] · Kun Wang[1] · Daofeng Mei[1] · Zhaojun Ma[1] · Chuguang Zheng[1]

Received: 13 February 2015 / Accepted: 25 June 2015 / Published online: 14 July 2015

Abstract Chemical looping with oxygen uncoupling (CLOU) is a promising technology due to its potential to reduce energy efficiency penalty and cost associated with CO_2 capture. In this work, a $CuO/CuAl_2O_4$ oxygen carrier (OC) prepared by sol–gel was investigated in its oxygen release kinetics ($4CuO \rightarrow 2Cu_2O + O_2$). Based on several well-organized temperature-programmed reduction experiments which were conducted in a thermogravimetric analyzer, the activation energy E (343.7 kJ mol^{-1}) and pre-exponential factor A (3.78×10^{12} s^{-1}) were determined and the Avrami–Erofeev random nucleation and subsequence growth model fitted well with the reduction experimental data. The enhancement of OC reduction rate in real fluidized bed CLOU reactor using different types of solid fuels (petroleum coke, anthracite, bituminous, and lignite) was identified in terms of the chemical kinetics and thermodynamics for the first time. It was found that the CuO reduction rate is more sensitive to the local temperature change than the oxygen concentration driving force. The results could contribute to the design, operation, and performance prediction of real CLOU reactors.

Keywords Reduction kinetics · Solid fuels · CLOU · Oxygen concentration driving force · Kinetics barrier

✉ Haibo Zhao
hzhao@mail.hust.edu.cn

[1] State Key Laboratory of Coal Combustion, Huazhong University of Science and Technology, Wuhan 430074, Hubei, People's Republic of China

Introduction

Chemical looping with oxygen uncoupling (CLOU) is a novel and attractive technology that allows the combustion of fossil fuels with inherent CO_2 separation [1, 2]. It utilizes a special oxygen carrier (OC) which is able to decompose to a reduced metal oxide and gas-phase oxygen in the fuel reactor (FR) and regenerate in the air reactor (AR). As a variant of chemical looping combustion (CLC), CLOU provides a possibility to accelerate fuel conversion by gaseous O_2 released from OC [3] and then attain lower solid circulation rate, smaller FR sizes, higher carbon conversion of solid fuels, higher CO_2 capture efficiency and higher combustion efficiency, especially for the combustion of solid fuels [4–7]. As shown in Fig. 1, a CLOU system typically involves two interconnected fluidized bed reactors with OC particles circulating between them. One of the reactors serves as the FR, in which the fuel is combusted with the help of gaseous oxygen supplied by the circulating OC. Then the reduced OC is regenerated by reaction with atmospheric oxygen in the AR.

A key requirement for the CLOU technology is that the OC can react reversibly with gas-phase O_2 at suitable temperatures and oxygen partial pressures. In principle, the capability of a certain material to release/uptake O_2 cyclically is first determined by its thermodynamic properties. Imtiaz et al. [8] summarized the thermodynamics and experimental studies concerning the development of the materials that are commonly used as OCs for CLOU, i.e., CuO/Cu_2O, Mn_2O_3/Mn_3O_4 and Co_3O_4/CoO. Among the monometallic oxides, the CuO/Cu_2O system has received considerable attention since it has some advantageous characteristics such as high oxygen transport capacity, stable recyclability of oxygen release and uptake, moderate price, being exothermic for fuel combustion in

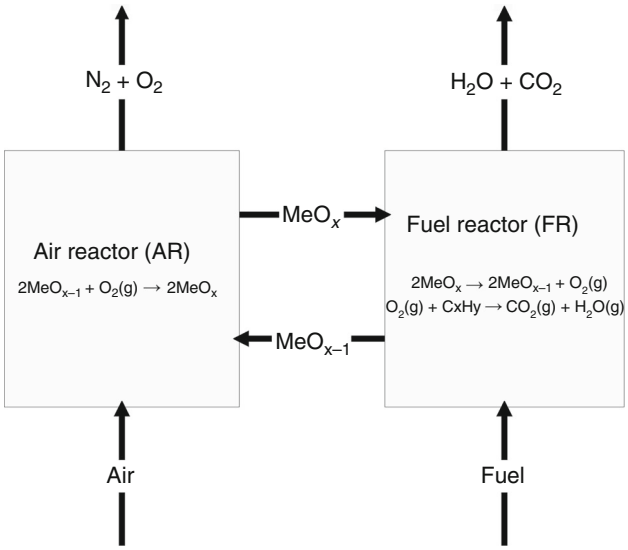

Fig. 1 Schematic of CLOU system

the FR, and being environmental friendly [9]. Usually, the active component CuO is supported by different inert supports of e.g., ZrO_2, $MgAl_2O_4$, Al_2O_3, SiO_2, MgO, TiO_2, and sepiolite [10], to withstand a higher temperature (such as 900–1000 °C). Zhao et al. [11] used both wet and dry impregnation methods to synthesize Cu-based OCs supported on Al_2O_3. They claimed that the OCs produced in this manner are suitable for multi-cycle tests. Later, Cui et al. [12] applied mechanic mixing, sol–gel, and wet impregnation methods to prepare Cu-based OCs supported on TiO_2. Test results indicated all prepared OCs functioned properly in the multi-cycles of reduction and oxidation (redox) in thermogravimetric under 800 °C. Moreover, they found that nucleation and diffusion models could better describe kinetics of prepared OC based on the sol–gel method. Mei et al. [13] have examined the CLOU reactivity of sol–gel-derived $CuO/CuAl_2O_4$ OCs (60 mass% CuO:40 mass% $CuAl_2O_4$) with different coals. It was found that using $CuO/CuAl_2O_4$ OC, which was able to release and absorb gaseous O_2 repeatedly at combustion temperatures (800–1000 °C) without agglomeration and sintering, could attain nearly complete conversion of coals in the FR. On the other side, a lot of CLOU work has recently been done on combined metal oxide as CLOU OCs. Ksepko et al. [14, 15] prepared bi-metallic Fe–Cu OCs and evaluated the performance of these carriers with hard coal/air. The effects of the OC chemical composition, particle size, and steam addition on the reaction rates were determined. Wu et al. [16] synthesized nanocrystalline $CuFe_2O_4$ and studied the kinetics of the thermal process using TG/DSC technique. Ryden et al. [9] provided an overview of the possibility to design feasible OC materials from combined oxides, i.e., oxides with crystal structures that include several different cations. They claimed that the combined oxides OC such as $(Mn_yFe_{1-y})O_x$ can release very substantial amounts of oxygen. When using this kind of OC, the overall reaction in the FR will be exothermic and the temperature of O_2 release can be controlled in some materials by altering the proportions between different components.

The knowledge of the kinetics of the reduction and oxidation reactions is essential for the design and process simulation of CLOU systems [17, 18]. It has been observed that the rate of CuO decomposition is slower than that of Cu_2O oxidation in the temperature range of interest to copper looping systems. Therefore, it is especially critical to well understand the decomposition rate for predicting the FR performance. The basic reaction and kinetic equations for CuO reduction (or decomposition here) process [19] are:

$$4CuO \rightarrow 2Cu_2O + O_2 \tag{1}$$

$$\frac{dX}{dt} = A \exp\left(-\frac{E}{RT}\right) f(X) \left(\frac{p_{O_{2,e}} - p_{O_2}}{p_{O_{2,e}}}\right)^{\kappa} \tag{2}$$

where A is the pre-exponential factor, R is the gas constant ($R = 8.314$ J mol^{-1} K^{-1}), E is the activation energy, and X is the conversion ratio. The term $f(X)$ is the reaction kinetics function. $p_{O_{2,e}}$ is the oxygen equilibrium partial pressure, p_{O_2} is the local oxygen partial pressure, and exponent κ is the reaction order on p_{O_2}. The thermogravimetric analysis (TG), which provides a well-conditioned reaction environment, was usually used for reaction kinetics analysis [17]. Because the reduction of cupric oxide is a thermal decomposition process and the external diffusion is ruled out by suitable gas flow rate in the TG, the value of κ becomes zero, generally. Eyring et al. [20] simulated the conditions of CLOU in TG, using pure CuO powder. The analysis showed the advantages of CLOU in providing rapid combustion of the carbon with carbon burnout times lower than the decomposition times of the OC. Song et al. [21] investigated the redox behavior of CuO/SiO_2 for the temperature range of 800–975 °C in a TG reactor. The reduction rate was found to increase gradually with temperature, while in contrast, a drop in the oxidation rate was observed. Wang et al. [22] determined the kinetics of Cu-based OCs by using distributed activation energy model by TG. The mechanism function is the nucleation and nuclei growth, and it is shown as $f(X) = 3(1 - X)[-\ln(1 - X)]^{2/3}$. However, the reduction kinetics of $CuO/CuAl_2O_4$ OC is still not reported. One objective of this study is to determine the reduction kinetics using TG.

Since the reaction environment in TG is far from the practical CLOU processes, the kinetic model obtained should be examined that whether it is suitable for the

reduction reaction in a fluidized bed reactor. It is well understood that the rates of reversible reactions such as the CuO–Cu_2O system [23] are affected by the difference between the actual and equilibrium concentrations of reacting species, the so-called oxygen concentration driving force. This has also been observed to occur in the CLOU regime with copper-based OCs.

Adánez-Rubio et al. [10] observed that an increase in the supplied partial pressure of oxygen can cause a decrease in the decomposition rate of CuO. They suggested that the decrease in the decomposition rate is ascribed to a decrease in the oxygen concentration driving force. On the other hand, due to the effect of temperature on the equilibrium partial pressure of oxygen as well as the reaction rate constant k of CuO decomposition $\left(k = A\exp(-\frac{E}{RT})\right)$, possible local temperature increase surrounding the OC particles, as a result of fuel combustion, also contributes to an increase in reduction rate. Sahir et al. [19] suggested that the apparent activation energy for CuO decomposition in the CLOU of Mexican Petcoke is contributed by the effects of both chemical kinetics and thermodynamics (partial pressure difference or oxygen concentration driving force). Clayton and Whitty [24] investigated decomposition of two different copper-based OCs to develop a universal kinetic expression to describe the observed rate of reaction as a function of temperature, conversion, and gas environment. These interacting factors make identification of kinetics of the CuO/$CuAl_2O_4$ reduction in the FR of CLOU challenging.

Another objective of this study is therefore to gain a better understanding of the reaction mechanisms associated with the reduction of CuO/$CuAl_2O_4$ in the fluidized bed FR. A series of CLOU experiments using petroleum coke (PC), GP coal (anthracite), FG coal (bituminous), and SL coal (lignite) as fuel were conducted at different temperatures in a batch fluidized bed reactor. Taking the effects of temperature and oxygen concentration into consideration, a new method (or idea) with the introduction of the reaction rate constant strengthen factor S_k and the oxygen concentration driving force strengthen factor S_o was developed to identify the kinetics of the CuO/$CuAl_2O_4$ reduction. The results could contribute to the analysis of kinetics for CuO–Cu_2O system as well as the design, operation, and performance prediction of real CLOU reactors.

Experimental

Oxygen carrier particles

The sol–gel process is used to prepare the Cu-based OC because it performs homogenous, controllable microstructure, high-purity, and accurate stoichiometry. Generally, there are four steps in the sol–gel procedure, i.e., the preparation of boehmite γ-AlOOH sol, the preparation of the γ-AlOOH wet gel, the drying of the wet gel, and the heat treatment (calcinations, 500 °C for 5 h and then 1050 °C for 10 h). The reagents used in the preparation of the CuO/$CuAl_2O_4$ OC are aluminum isopropoxide [$Al(C_3H_7O)_3$, KESHI Co., 99.9 % purity], copper nitrate [$Cu(NO_3)_2{\cdot}3H_2O$, Sinopharm Co., 99.9 % purity], and nitric acid (1 mol L^{-1}), where the copper nitrate and the aluminum isopropoxide are precursors for Cu and Al elements in the OC, and nitric acid is the catalyst for homogenization. A higher CuO content may lead to sintering while a lower CuO content will result in a lower active oxygen capacity. The designed mass ratio in the OC is 60 mass% CuO and 40 mass% $CuAl_2O_4$. The comprehensive performance of CuO/$CuAl_2O_4$ with the ratio 60/40 mass% has been identified the best before [13]. The target OC particles are those in the diameter of 0.10–0.30 mm.

Fuel particles

Petroleum coke, GP coal (anthracite), FG coal (bituminous), and SL coal (lignite) were used in the CLOU experiments in a batch-operated fluidized bed reactor. The coals were first dried under 105 °C for 10 h in an oven and then ground and sieved to produce particles with a diameter range of 0.20–0.30 mm. The final particles were then stored in a drying basin ready for use. The proximate and elemental analysis of the fuels was determined by an ultimate analyzer (Vario, EL-2) and a proximate analyzer (Las Navas, TG2000). The results are displayed in Table 1.

TG experiments

Kinetic experiments were performed in a TG (WCT-1D). To evaluate reaction kinetics, it was important to ensure that all transport limitations (heat and mass) were absent. A series of experiments were carried out first to obtain suitable mass sample, particle size, and gas flow rate. As a result, the gas flow rate, loading mass, and particle size were optimized as approximately 60 mL min^{-1}, 28 mg, and 0.10–0.30 mm, respectively. The Cu-based OC particles were then heated from room temperature to 1000 °C with heating rates of 3, 5, 10, and 20 °C min^{-1} to analyze the reduction kinetics. Nitrogen was used as carrier gas during the reduction period. In the oxidation periods, air was introduced to re-oxidize the OC.

The reduction–oxidation continuous cyclic operation of 10 mg OC was conducted at atmospheric pressure to determine the stability of OC in TG. The cyclic temperature for reduction and oxidation was selected as 950 °C. Nitrogen with a flow rate of 60 mL min^{-1} was used as carrier gas during the 20-min reduction period. In the

Table 1 Proximate and ultimate analysis of the fuels

	Proximate/mass%, ad				Ultimate/mass%, ad				Low heating value/MJ kg^{-1}
	Moisture	Volatiles	Ash	FC	C	H	N	S	H_L
PC	0.58	9.11	0.20	90.11	86.59	3.81	1.27	6.26	34.97
GP	2.25	10.69	20.62	66.44	70.04	3.54	1.90	1.24	26.17
FG	1.65	27.19	19.62	51.54	65.54	3.34	1.24	0.80	28.85
SL	8.62	41.59	35.47	14.32	48.33	4.11	0.85	0.48	12.82

oxidation periods, air was introduced to re-oxidize the OC for 16 min.

Fluidized bed experiments

The CLOU experiments were carried out in a batch fluidized bed reactor. As shown in Fig. 2, the reactor mainly consists of the gas control unit, the reaction unit, and the gas detection unit. The gas control unit provides air or N_2 as the fluidization gas to simulate the AR or FR atmosphere in the CLOU. The fluidization gas is introduced into the reactor from the bottom. The reaction unit includes a stainless reaction tube with a length of 892 mm and a diameter of 26 mm placed into an electrical furnace. A porous plate is placed in the tube at 400 mm from the bottom. The reactor temperature is measured by a type K thermocouple at about 10 mm above the porous plate. OC particles and fuel particles were introduced into the reactor through the hopper on the top of the reactor. All gaseous products exiting the reactor were first led to an electric cooler to remove the steam. The gas was then led to an on-line gas analyzer (Gasboard Analyzer 3100) to measure the concentrations of CO_2, CO, CH_4, H_2, and O_2.

The simulated CLOU processes using four different solid fuels and $CuO/CuAl_2O_4$ as OC were investigated in the fluidized bed reactor under cyclic air atmosphere (simulating the AR) and N_2 atmosphere (simulating the FR). Before each test, 40 g OCs were exposed to air atmosphere at a set-point temperature for 30 min, ensuring its full oxidation. Following that, the fluidization gas with a flow rate of 800 mL min^{-1} (the inlet gas velocities were 4–9 times the minimum fluidization velocity) was fast switched to N_2, resulting in a sharp decrease in the O_2 partial pressure. When the O_2 partial pressure decreases to be lower than the corresponding equilibrium partial pressure of the OC at the set-point temperature, the OCs decompose and produce gaseous O_2 continuously. Once a stable oxygen concentration was achieved, 0.3 g fuel particles with diameters of 0.20–0.30 mm were added into the hopper and pushed into the reactor by a pressurized purging nitrogen gas. The fuel was assumed to be completely burnt out until no CO_2 was detected in the exhaust gas. Afterward, the fluidization gas was switched to air to regenerate the reduced OCs.

Data evaluation

Oxygen carrier conversion

In the TG experiments, reactivity data were obtained through analyzing the mass variations of reduction

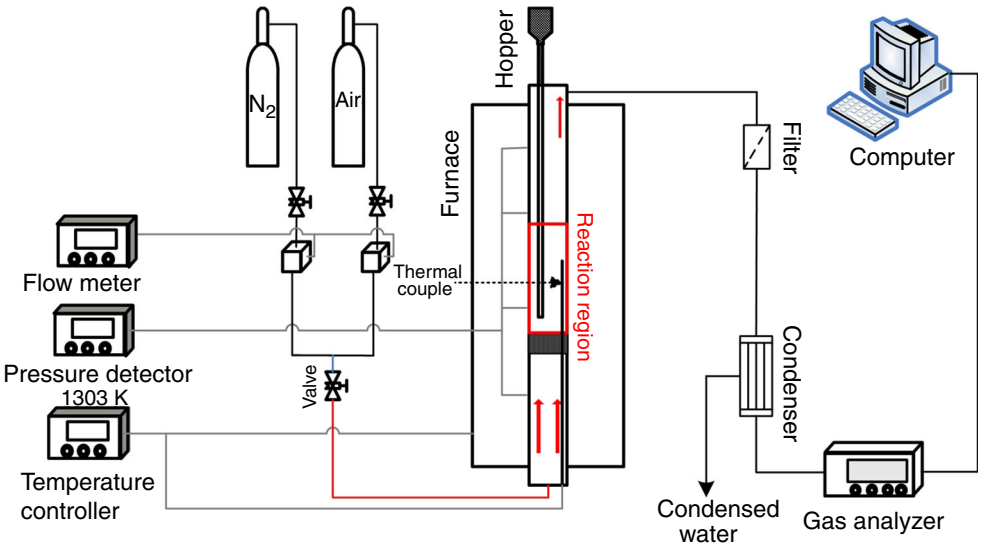

Fig. 2 Overview of the fluidized bed reaction system

reactions. The OC conversion (X_{OC}) can be calculated according to Eq. (3):

$$X_{OC} = \frac{m_{ox} - m}{m_{ox} - m_{red}} \tag{3}$$

where m is the mass of the sample at each time, m_{ox} is the mass of the sample fully oxidized, and m_{red} is the mass of reduced sample.

In the CLOU of PC and coals, the rate of oxygen generation of OC, x_{O_2}, was calculated through the oxygen balance in the reactor [25]:

$$x_{O_2} = F_{O_2} + F_{CO_2} + 0.5(F_{CO} + F_{H_2o}) - 0.5F_{O,coal} \tag{4}$$

where F_i is the molar gas flow of each component exiting the FR, which is calculated as

$$F_i = F_{flus} \cdot y_i \tag{5}$$

where y_i is the molar fraction of the component i (include O_2, CO_2, CO, CH_4, or H_2) in the product gas. F_{flus} is the molar flow rate of the gas in the outlet, determined by N_2 balance between the inlet and the outlet of the reactor. The water concentration was not measured in the experiment. Therefore, in order to consider the oxygen exiting with H_2O coming from oxidation of hydrogen in the solid fuels, it was assumed that that the hydrogen evolution was proportional to the carbon evolution, maintaining the same C/H ratio in the gases than in the solid fuels. However, because a little of methane and hydrogen were detected in the experiment, the H_2O flow was calculated as

$$F_{H_2O} = 0.5f_{H/C}(F_{CO_2} + F_{CO} + F_{CH_4}) - (F_{H_2} + 2F_{CH_4}) \tag{6}$$

where $f_{H/C}$ is the hydrogen-to-carbon molar ratio in the solid fuels (0.607 for GP coal, 0.612 for FG coal, 1.020 for SL coal, and 0.528 for PC). Similarly, the evolution of oxygen from fuel was assumed to be proportional to fuel evolution. Thus, the flow of oxygen coming from fuel was calculated as

$$F_{O,coal} = f_{O/C}(F_{CO_2} + F_{CO} + F_{CH_4}) \tag{7}$$

where $f_{O/C}$ is the oxygen-to-carbon molar ratio in the fuels (0.004 for GP coal, 0.089 for FG coal, 0.033 for SL coal, and 0.018 for PC).

Therefore, the OC conversion in the fluidized bed for reduction reaction, X_{red}, can be calculated from the integration of x_{O_2} with time.

$$X_{red} = \frac{1}{n_{O_2}} \int_{t_0}^{t} x_{O_2} \mathrm{d}t \tag{8}$$

where n_{O_2} (mol) is the moles of gaseous O_2 which can be released from fully oxidized CuO/$CuAl_2O_4$ OC. For the reaction kinetics analysis, the OC conversion was normalized within 0–1 based on the actual total oxygen amounts.

Kinetic analysis based on TG experiments

The isoconversional (model-free) method, which uses the principle that the reaction rate at a constant extent of conversion is only a function of temperature, is one of the most common methods used to determine the activation energy without assuming the reaction kinetics function in advance. As mentioned in the introduction, κ becomes zero since the oxygen driving force is ruled out for a thermal decomposition process in TG. Thus, Eq. (2) can be converted to Eq. (9) for a constant heating rate/non-isothermal conditions:

$$\frac{\mathrm{d}X}{\mathrm{d}T} = \frac{A}{\beta} \exp\left(-\frac{E}{RT}\right) f(X) \tag{9}$$

where β is the heating rate. $G(X)$ is the integral expression of $f(X)$:

$$G(X) = \int_0^X \frac{1}{f(X)} \mathrm{d}X = \frac{A}{\beta} \int_0^T \exp\left(-\frac{E}{RT}\right) \mathrm{d}T = \frac{AE}{\beta R} P(\mu) \tag{10}$$

$$P(\mu) = \int_{\mu_T}^{\infty} \frac{\exp(-\mu)}{\mu^2} \mathrm{d}\mu \tag{11}$$

$P(\mu)$ is the Arrhenius temperature integral, where $\mu = E/(RT)$. However, the analytical value of $P(\mu)$ cannot be integrated. The MKN, Tang, and Starink approximation formulas are the best-known, most cited, and most accurate approximations for temperature integral. Moreover, the Starink approximation has been approbated by the ICTAC kinetics committee [26]. In this paper, the Starink approximation is used to calculate the activation energies. It is based on a two-term approximate formula, which has the following general form [27]:

$$\ln \frac{\beta}{T^{1.8}} = -1.0070 \left(\frac{E}{RT}\right) + C \tag{12}$$

where C is a constant. The trends of $\ln(\beta T^{-1.8})$ and T^{-1} must be linear according to Eq. (12).

The reduction reaction of OC can be described using a single mechanism function. Some normally used $f(X)$ expressions are summarized in Table 2. The Satava method [28] is adopted to infer the most probable mechanism function. Equation (13) can be obtained by Doyle approximation [29]:

$$\lg[G(X)] = \lg\left(\frac{AE}{\beta R}\right) - 2.315 - 0.4567 \frac{E}{RT} \tag{13}$$

Under a constant heating rate (in an non-isothermal experiment), $\lg[G(X)]$ has a linear relation with $1/T$. The $G(X)$ functions with good linear relation with $1/T$ can be screened out.

Table 2 [22, 30] Usually used mechanism functions: integral expression $G(X)$ and differential expression $f(X)$

Number	Reaction model	$G(X)$	$f(X)$
1–2	Jander function	$[1-(1-X)^{1/2}]^n$ ($n = 1/2, 2$)	Depending on $[1-(1-X)^{1/2}]^n$
3	Z–L–T function	$[(1+X)^{-1/3}-1]^2$	$3/2(1-X)^{4/3}[(1-X)^{-1/3}-1]^{-1}$
4–14	Avrami–Erofeev	$[-\ln(1-X)]^n$ ($n = 1/4, 1/3, 2/5, 1/2, 2/3, 3/4, 1, 3/2, 2, 3, 4$)	Depending on $[-\ln(1-X)]^n$
15	P–T function	$\ln[(1-X)/X]$	$X(1-X)$
16–21	Mampel	X^n ($n = 1/4, 1/3, 1/2, 1, 3/2, 2$)	Depending on X^n
22–27		$1-(1-X)^n$ ($n = 1/4, 1/3, 1/2, 2, 3, 4$)	Depending on $1-(1-X)^n$
28–29		$(1-X)^{-n}$ ($n = 1, 1/2$)	Depending on $(1-X)^{-n}$
30–31	Index law	$\ln X^n$ ($n = 1, 2$)	Depending on $\ln X^n$

Results and discussion

Effect of heating rate and cyclic experiments

TG experiments with the heating rates of 3, 5, 10, and 20 °C min^{-1} were carried out. Figure 3 shows the mass loss and reaction rate curves of the OC under different heating rates. It was observed that the start and end points of oxygen releasing and absorbing regions move forward to high temperature with an increasing heating rate. The reason is that the OC particles can reach the minimum reaction temperature more easily at a low heating rate. In addition, the peak reaction rate also increases as the heating rate, which illustrates that high temperature is helpful for the reduction reaction. Because of the thermal lag, the peaks of DTG also move forward to high temperature. The heating rate has little effect on the final mass loss and mass gain. The durability and thermal stability of OC were also investigated through a 20-cycle redox operation at 900 °C. The times for reduction and oxidation reactions were both 20 min. It was found that the relativities of oxygen releasing and adsorbing are stable during the cycles. The degradation of $CuO/CuAl_2O_4$ particle is negligible.

Reaction mechanism description

Based on the experimental data obtained and the approximation, trends of $\ln(\beta T^{-1.8})$ and T^{-1} under different X values (0.1–0.4) are shown in Fig. 4. It should be noted that the OC conversion of 0.1–0.4 is from the decomposition of CuO. The decomposition of $CuAl_2O_4$, which is much slower than that of CuO [31], has a negligible oxygen contribution and it does not affect the kinetics mechanism. This is confirmed by the fact that the mass loss results in Fig. 3 are below the

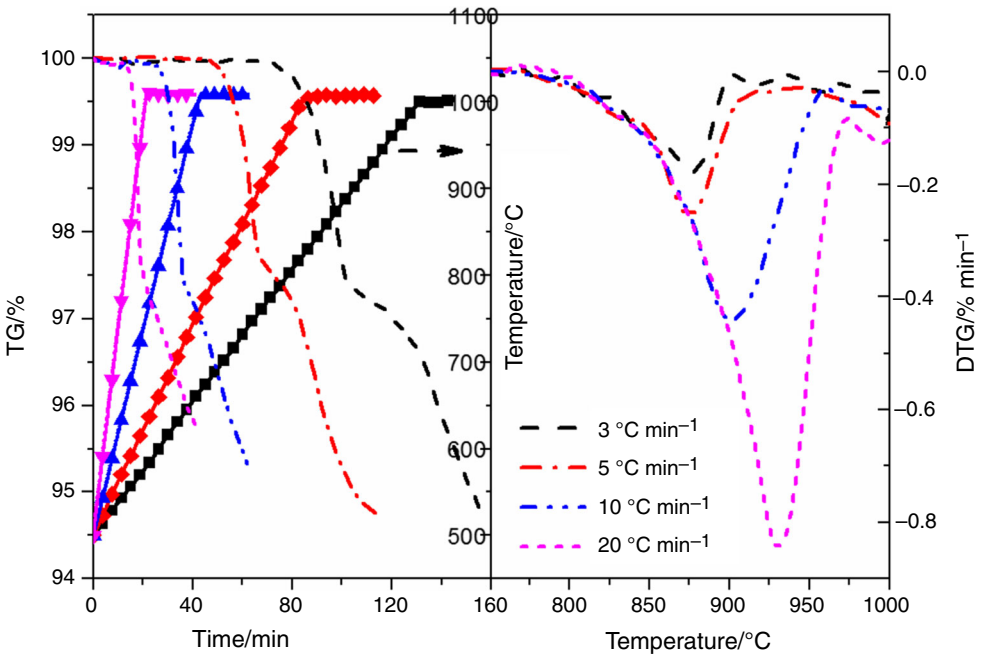

Fig. 3 Mass loss and reaction rate curves of the OC under different heating rates for reduction

theoretical value for an OC with 60 % CuO. The values of E shown in Table 3 could be obtained by applying linear regression of the slopes. The distributed average activation energy of CuO/$CuAl_2O_4$ for reduction obtained is 343.7 kJ mol^{-1}. The value is close to the reported activation energy values of 322 kJ mol^{-1} and 327 kJ mol^{-1} obtained from TG experiments for pure CuO particles of the size range 10–20 and 1–10 μm, respectively [22].

As known, by fitting linearly the set (lg[$G(X)$], T^{-1}), the linear correlation coefficient, r, is obtained as shown in Table 4. The Avrami–Erofeev model (AEM) which has been used in several works [22, 32] to develop the rate equation is confirmed to be the most probable $G(X)$. The $f(X)$ function is then expressed as a function of conversion: $f(X) = n(1 - X)[-\ln(1 - X)]^{(n-1)/n}$, where n ($n = 2/3$) is the Avrami exponent indicative of the reaction mechanism and crystal growth dimension.

Once the activation energy E and mechanism function $G(X)$ are determined, the pre-exponential factor (A) can be calculated through linear fitting $G(X)$ and $EP(\mu)$ $(\beta R)^{-1}$ as shown in Eq. (10). Figure 5 shows the trends of $G(X)$ and $EP(\mu)$ $(\beta R)^{-1}$ under different heating rates. The linear relationships of $G(X)$ and $EP(\mu)$ $(\beta R)^{-1}$ under different heating rates are high especially for higher heating rates, meaning a reasonable estimation to A. Table 5 shows the calculated values of A, and the average value of A is 3.78×10^{12} s^{-1}.

Using the activation energy, the mechanism function and pre-exponential factor obtained, the kinetic model of CuO/$CuAl_2O_4$ could be established, as follows:

$$\frac{dX}{dt} = 5.67 \times 10^{12} \exp\left(-\frac{4.1 \times 10^4}{T}\right)(1 - X)\,[-\ln(1 - X)]^{1/3} \quad (14)$$

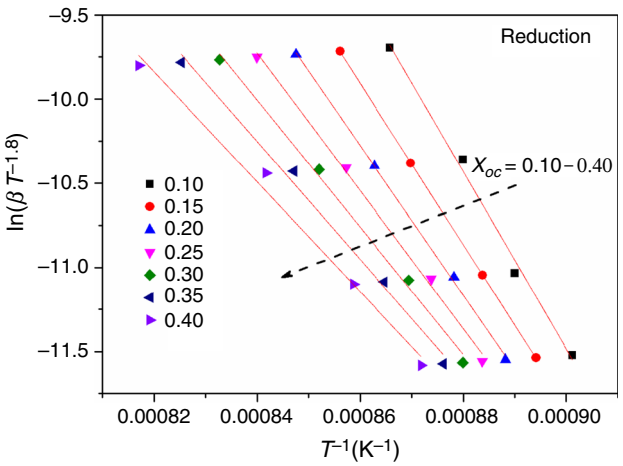

Fig. 4 Trends of $\ln(\beta T^{-s})$ and T^{-1} under different conversions(X) of oxygen carrier

Analysis of oxygen release in fluidized bed reactors

The oxygen release mechanism determined by TG is suitable in wide temperature range at the ideal condition. However, in the fluidized bed reactor of real CLOU system, the mechanism may be not suitable for the actual reduction reaction since the change in the temperature and oxygen concentration driving force. Obviously, the reaction order κ in Eq. (2) is no longer zero during the oxygen release in the fluidized bed reactor. Assuming a first-order [28] dependence on p_{O_2} [32], the OC reduction rate has been analyzed by the following general form:

$$\frac{dX}{dt} = 5.67 \times 10^{12} \exp\left(-\frac{4.1 \times 10^4}{T}\right)(1 - X)\,[-\ln(1 - X)]^{1/3}\left(\frac{p_{O_2,e} - p_{O_2}}{p_{O_2,e}}\right) \quad (15)$$

Taking the variation of p_{O_2} along the bed height into consideration, the arithmetic mean of the O_2 partial pressure driving forces at the inlet and outlet is used. The inlet oxygen partial pressure $p_{O_2,in}$ is zero for the FR stage of the experiments, and the outlet partial pressure $p_{O_2,out}$ is obtained from the experimental data. Then, the oxygen driving force can be expressed as [19]:

$$f(p_{O_2}) = \left(\frac{p_{O_2,e} - p_{O_2}}{p_{O_2,e}}\right)_{avg} = \frac{(p_{O_2,e} - p_{O_2,in}) + (p_{O_2,e} - p_{O_2,out})}{2p_{O_2,e}} = \frac{2p_{O_2,e} - p_{O_2,out}}{2p_{O_2,e}} \quad (16)$$

$p_{O_2,e}$ is determined by the Gibbs free energy as [21]:

$$p_{O_2,e} = \exp\left(-\frac{\Delta G}{RT_{avg}}\right) \quad (17)$$

In this work, the Gibbs free energy, ΔG, is derived on the basis of the empirical equation developed by Kubaschewski et al. [33] for cupric oxide decomposition:

$$\Delta G = 292 + 0.051T_{avg} \times \lg T_{avg} - 0.37T_{avg}\,(298 \le T_{avg} \le 1323\text{K}) \quad (18)$$

In the CLOU experiments, fuel particles were added into the fluidized bed reactor through the hopper on the top of the reaction tube. As an example, Fig. 6 presents the dry outlet gas concentrations as a function of time for a reduction and oxidation period using PC as fuel at 950 °C. The oxygen concentration kept stable until the coke was added into the reactor and combusts with the gaseous O_2. There was an obvious decrease in O_2 concentration and a sharp increase in CO_2 concentration. The CO_2 concentration reached its maximum about 50 s later, then decreased sharply to zero within 55 s because the PC particles were

Table 3 Values of E at different conversions X_{OC}

X_{OC}	0.10	0.15	0.20	0.25	0.30	0.35	0.40	Average
E/kJ mol^{-1}	435.27	395.24	366.27	337.94	312.14	289.48	269.59	343.71
r	0.9969	0.9999	0.9996	0.9987	0.9980	0.9969	0.9950	

Table 4 Relation coefficients (r) for the most probable mechanism functions $G(X)$

$G(X)$	r at 3 °C min^{-1}	r at 5 °C min^{-1}	r at 10 °C min^{-1}	r at 20 °C min^{-1}	Average r
$[-\ln(1-X)]^{2/3}$	0.9986	0.9896	0.9988	0.9916	0.9947
$1-(1-X)^{1/4}$	0.9982	0.9886	0.9985	0.9906	0.9940
$1-(1-X)^{1/3}$	0.9981	0.9882	0.9983	0.9903	0.9938
$[1-(1-X)^{1/2}]^{1/2}$	0.9978	0.9875	0.9981	0.9896	0.9933

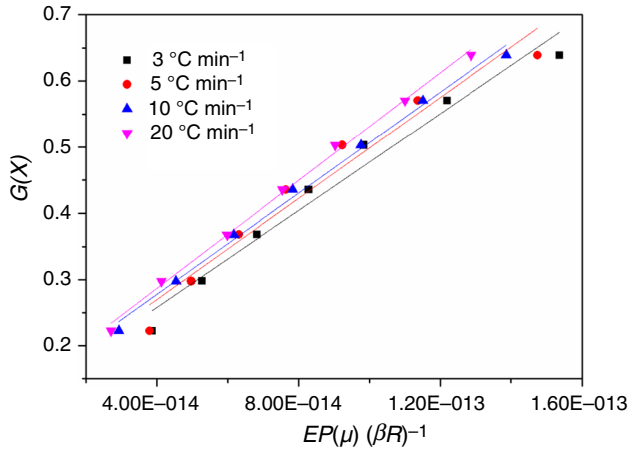

Fig. 5 Trends of $G(X)$ and $EP(\mu)\ (\beta R)^{-1}$ under different heating rates

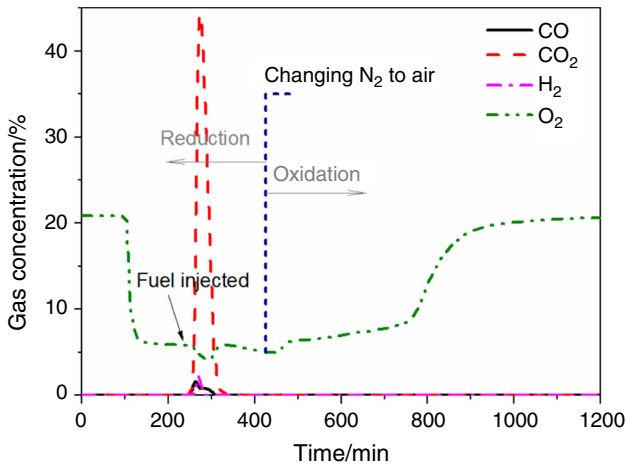

Fig. 6 Gas concentration profiles in a reduction and oxidation at 950 °C using petroleum coke as fuel

Table 5 Calculated values of A ($\times 10^{12}$ s^{-1})

	Heating rate/°C min^{-1}				Average
	3	5	10	20	
A	3.61	3.78	3.75	3.99	3.78
r	0.9941	0.9899	0.9997	0.9993	–

burnt out. Small amounts of CO and H_2 were detected in the beginning of the reduction period, which was due to the devolatilization of the coke. The volatiles released from the coke did not have enough time to react with the gaseous O_2 before leaving the reactor. In the following oxidation period, no carbon-containing gases were observed in the reactor outlet, indicating that all of the PC was converted and no carbon deposits on the surface of OC particle in the reduction period.

The OC conversion X_{red} can be calculated by Eq. (8) using the experimental data. The dots of different shapes in Fig. 7 represent the OC conversions as a function of time at different temperatures. Taking the experimental data of using PC as fuel for example, Fig. 7a includes three time periods: the first phase (0 ∼ ca. 65 s) when OC particles are introduced in N_2, represented by an initial slope of a lower magnitude, and the second phase (ca. 65 s ∼ ca. 120 s) where fuels are introduced in the reactor, represented by a slope of higher magnitude, and the last phase (>ca. 120 s) when fuels are burnt out and the slope of OC conversion curve returns to that of the first phase. It is found that Eq. (14) could roughly predict the experimental OC conversion curves in the first time period and the last time period (when no fuel is available). However, the difference in the magnitudes of slopes occurs once fuel is introduced, because the rate of OC reduction reaction is enhanced due to the increase in temperature and the removal of O_2 by combustion. The changing trends of OC conversion with time for the reduction by GP, FG, and SL coal are similar to that of PC.

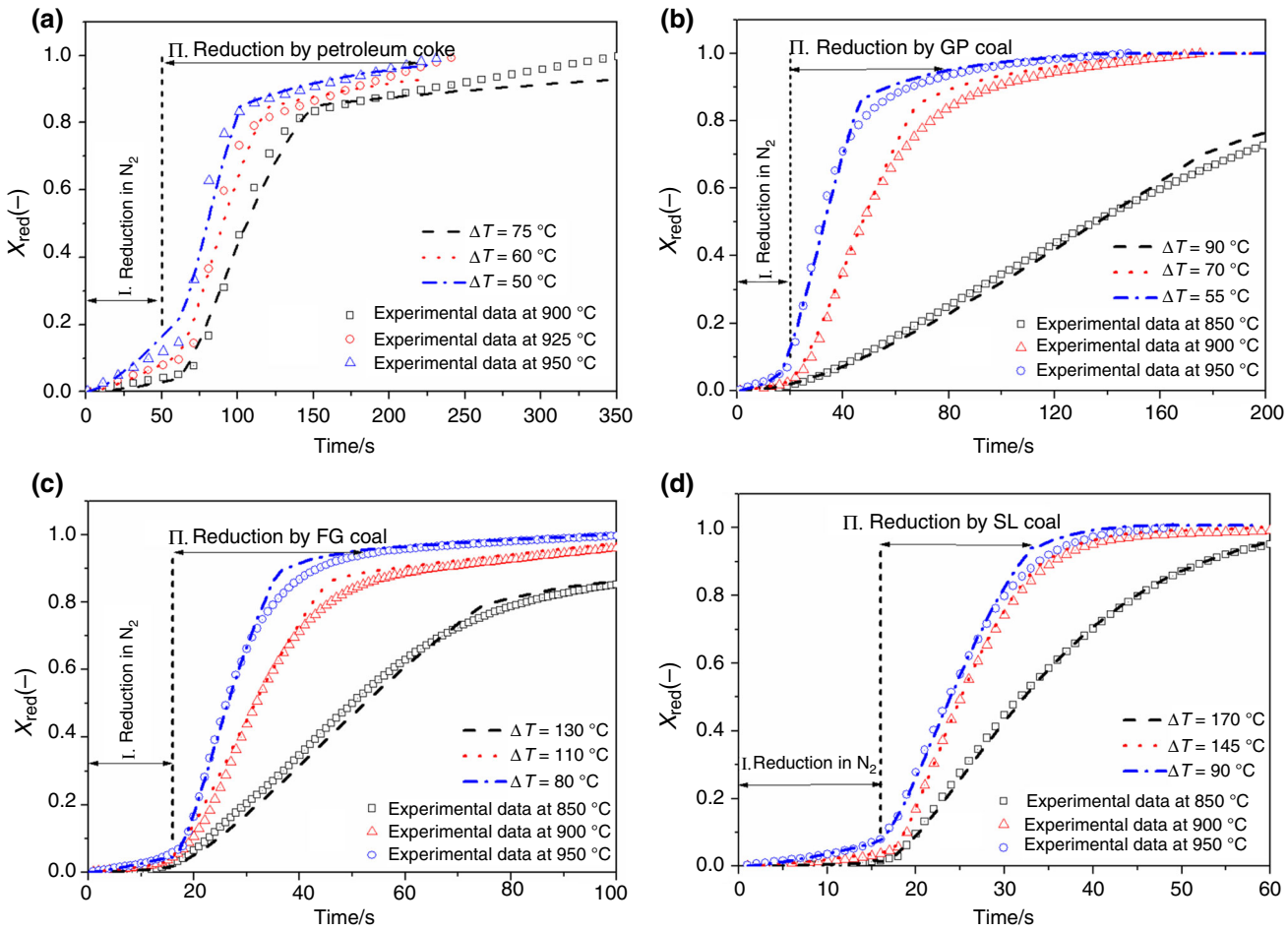

Fig. 7 Comparison of experimental data and fitting by Eq. (15) with temperature amending during the period reduction by PC, GP, FG, and SL coal

Accounting for the temperature increase due to the combustion, Eq. (15) can be amended by temperature ΔT to fit the second phase of experimental data as the dash lines shown in Fig. 7. At first, an amending temperature is assumed, and the change in the oxygen equilibrium partial pressure is calculated by Eq. (17). Then the Newton's iteration method is used to determine the actual amending temperature through matching the experimental results well, in which the reduction rate Eq. (15) is solved by the finite-difference method. It can be seen that the amending temperatures decrease with the reactor temperature increases. With respect to different solid fuels, the OC conversion rates become from slow to fast in the order of PC, GP, FG, and SL coal which correspond to the order of the volatile content in the four kinds of solid fuels. One reason may be that oxygen consumption is much faster for high-volatile-content fuel, resulting in the stronger oxygen driving force. Another reason may be a higher volatile in solid fuel contributes to a higher local temperature increase (due to the exothermic combustion), which leads to a higher reaction rate constant k and a higher oxygen equilibrium partial pressure.

Usually, temperature plays two roles in the determination of reaction rates: First, it shows up in the exponential function $(k = A\exp(-\frac{E}{RT}))$; second, it affects the oxygen concentration driving force, which is a function of temperature due to the equilibrium partial pressure of oxygen. The interacting factors make identification of kinetics of the $CuO/CuAl_2O_4$ reduction in the FR of CLOU challenging. To describe the reaction mechanism better, the reaction rate constant strengthen factor S_k and the oxygen concentration driving force strengthen factor S_o are defined:

$$S_k = \frac{k_{T+\Delta T}}{k_T} = \exp\left[\frac{E}{R}\left(\frac{1}{T} - \frac{1}{T+\Delta T}\right)\right] \tag{19}$$

$$S_o = \frac{f_{T+\Delta T}(p_{O_2})}{f_T(P_{O_2})} \tag{20}$$

where T is the set temperature of experiment, ΔT is the amending temperature. The values of S_k and S_o are

Table 6 Reaction rate constant strengthen factor S_k and the oxygen concentration driving force strengthen factor S_o

Experiment temperature/°C	Factor S_k				Factor S_o			
	PC	GP	FG	SL	PC	GP	FG	SL
850	–	15.00	44.12	121.38	–	1.79	1.99	2.00
900	8.17	7.16	20.01	46.73	1.66	1.60	1.99	1.99
925	5.11	–	–	–	1.54	–	–	–
950	3.73	4.23	7.83	9.95	1.70	1.86	1.95	1.99

PC, GP, FG, and SL denote petroleum coke, anthracite, bituminous, and lignite, respectively

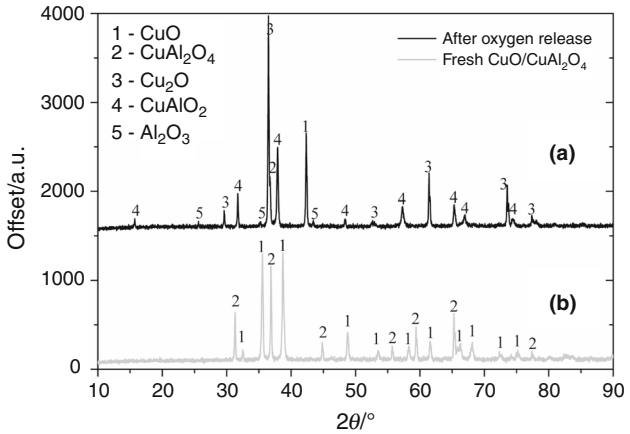

Fig. 8 XRD analysis of fresh and oxygen released oxygen carriers

displayed in Table 6. It can be seen that S_k is always larger than S_o, especially for low temperatures (S_k is 8–60 times larger than S_o) and high-volatile fuels (S_k is 5–60 times larger than S_o). It means that the OC conversion rate in the FR is mainly attributed to the local temperature increase, i.e., the reaction kinetics barrier is easier to overcome than the thermodynamics barrier, which agrees well with the results of Sahir et al. [19]. Thus, it can be concluded that the reduction rate is more sensitive to the local temperature change than the oxygen concentration driving force.

Characterization of OCs

The composition of the OC prepared is determined by Shimazu Cu target X-ray diffraction type XRD-7000, using maximum voltage 40 kV, maximum current 30 mA, scanned area 10°–90°. Fresh OC XRD diffraction pattern is shown in Fig. 8b. The main phases are CuO and $CuAl_2O_4$ without Al_2O_3 phase appearing, which indicates that the Al_2O_3 phase has combined with CuO into spinel $CuAl_2O_4$ compounds. As shown in Fig. 8a, the composition of the decomposed OC under N_2 atmosphere is composed of Cu_2O, $CuAl_2O_4$, $CuAlO_2$, and Al_2O_3 (minor phase). Obviously, CuO is fully decomposed to Cu_2O. $CuAlO_2$ and

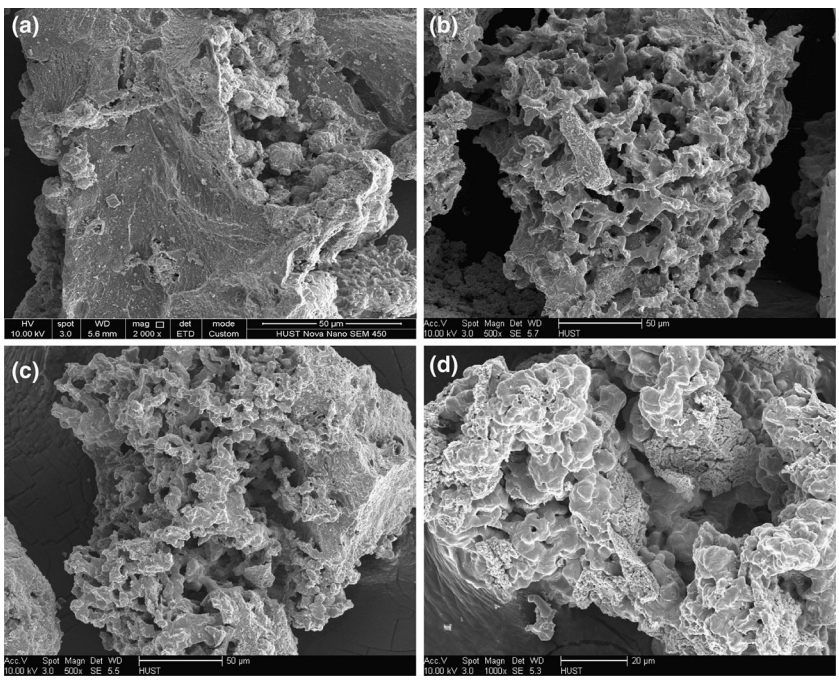

Fig. 9 Microstructure of OCs **a** fresh OC, **b** OC reacted with GP coal at 950 °C, **c** OC reacted with FG coal at 950 °C, **d** OC reacted with SL coal at 950 °C

Al_2O_3 are from the decomposition of $CuAl_2O_4$. However, the $CuAl_2O_4$ decomposition is incomplete.

The surface morphology of the OC particles was examined in an environment scanning electron microscope (ESEM, FEI Quanta 200). Figure 9 shows the SEM images of OC particles both fresh and after used. Obvious sintering was observed for the used OC with lignite. It can be inferred that a fuel with higher volatile leads to a higher local temperature increase (and then more serious sintering). Therefore, the temperature in the FR should be relatively lower for high-volatile fuels and relatively higher for low-volatile fuels.

Conclusions

In this paper, the kinetics and mechanism of the reduction reaction of a new CuO/$CuAl_2O_4$ OC (60 mass% active CuO) in CLOU were reported. Based on several well-organized temperature-programmed reduction experiments conducted in a TG, the distributed activation energy model was utilized to determine the activation energy E and pre-exponential factor A ($E = 343.7$ kJ mol^{-1}, $A = 3.78 \times 10^{12}$ s^{-1}). The suitable mechanism function was identified to be the Avrami–Erofeev random nucleation and subsequence growth model ($f(X) = 3/2(1 - X)[-\ln(1 - X)]^{1/3}$). Additionally, the enhancement of OC reduction rate in a fluidized bed CLOU reactor using different types of solid fuels was identified in terms of the chemical kinetics and thermodynamics for the first time. It was found that the rate of CuO/$CuAl_2O_4$ reduction was enhanced in the CLOU of solid fuels due to the removal of O_2 and the increase in local temperature surrounding the OC particles by the exothermic combustion of solid fuels with released O_2. The reaction rate constant strengthen factor S_k and the oxygen concentration driving force strengthen factor S_o were introduced to identify the intrinsic kinetics of the CuO/$CuAl_2O_4$ reduction. S_k is always larger than S_o, especially for low temperatures and high-volatile fuels. It means that the reaction kinetics barrier is easier to overcome than the thermodynamics barrier.

Acknowledgements This research was funded by "National Natural Science Foundation of China (51390494) and 51561125001." Meanwhile, the staffs from the Analytical and Testing Center and Huazhong University of Science and Technology are also appreciated for the related experimental analysis.

References

1. Adánez J, Abad A, Garcia-Labiano F, Gayan P, de Diego LF. Progress in chemical-looping combustion and reforming technologies. Prog Energy Combust. 2012;38(2):215–82.
2. Mattisson T. Materials for chemical-looping with oxygen uncoupling. ISRN Chem Eng. 2013;. doi:10.1155/2013/526375.
3. Leion H, Mattisson T, Lyngfelt A. Chemical looping combustion of solid fuels in a laboratory fluidized-bed reactor. Oil Gas Sci Technol. 2011;66(2):201–8. doi:10.2516/Ogst/2010026.
4. Mattisson T, Lyngfelt A, Leion H. Chemical-looping with oxygen uncoupling for combustion of solid fuels. Int J Greenh Gas Control. 2009;3(1):11–9.
5. Mattisson T, Leion H, Lyngfelt A. Chemical-looping with oxygen uncoupling using CuO/ZrO_2 with petroleum coke. Fuel. 2009;88(4):683–90. doi:10.1016/j.fuel.2008.09.016.
6. Abad A, Adánez-Rubio I, Gayan P, Garcia-Labiano F, de Diego LF, Adánez J. Demonstration of chemical-looping with oxygen uncoupling (CLOU) process in a 1.5 kW(th) continuously operating unit using a Cu-based oxygen-carrier. Int J Greenh Gas Control. 2012;6:189–200. doi:10.1016/j.ijggc.2011.10.016.
7. Adánez-Rubio I, Abad A, Gayan P, de Diego LF, Garcia-Labiano F, Adánez J. Performance of CLOU process in the combustion of different types of coal with CO_2 capture. Int J Greenh Gas Control. 2013;12:430–40.
8. Imtiaz Q, Hosseini D, Müller CR. Review of oxygen carriers for chemical looping with oxygen uncoupling (CLOU): thermodynamics, material development, and synthesis. Energy Technol. 2013;1(11):633–47.
9. Rydén M, Leion H, Mattisson T, Lyngfelt A. Combined oxides as oxygen-carrier material for chemical-looping with oxygen uncoupling. Appl Energy. 2014;113:1924–32.
10. Adánez-Rubio I, Arjmand M, Leion H, Gayan P, Abad A, Mattisson T, et al. Investigation of combined supports for Cu-based oxygen carriers for chemical-looping with oxygen uncoupling (CLOU). Energy Fuels. 2013;27(7):3918–27. doi:10.1021/ef401161s.
11. Zhao H-Y, Cao Y, Orndorff W, Pan W-P. Study on modification of Cu-based oxygen carrier for chemical looping combustion. J Therm Anal Calorim. 2013;113(3):1123–8.
12. Cui Y, Cao Y, Pan W-P. Preparation of copper-based oxygen carrier supported by titanium dioxide. J Therm Anal Calorim. 2013;114(3):1089–97. doi:10.1007/s10973-013-3131-2.
13. Mei DF, Zhao HB, Ma ZJ, Zheng CG. Using the sol–gel-derived CuO/$CuAl_2O_4$ oxygen carrier in chemical looping with oxygen uncoupling for three typical coals. Energy Fuels. 2013;27(5):2723–31. doi:10.1021/ef3021602.
14. Ksepko E, Labojko G. Effective direct chemical looping coal combustion with bi-metallic Fe–Cu oxygen carriers studied using TG-MS techniques. J Therm Anal Calorim. 2014;117(1):151–62. doi:10.1007/s10973-014-3674-x.
15. Ksepko E, Sciazko M, Babinski P. Studies on the redox reaction kinetics of Fe_2O_3–CuO/Al_2O_3 and Fe_2O_3/TiO_2 oxygen carriers. Appl Energy. 2014;115:374–83.
16. Wu X, Zhou K, Wu W, Cui X, Li Y. Magnetic properties of nanocrystalline $CuFe_2O_4$ and kinetics of thermal decomposition of precursor. J Therm Anal Calorim. 2013;111(1):9–16. doi:10.1007/s10973-011-2104-6.
17. Abad A, Garcia-Labiano F, de Diego LF, Gayan P, Adánez J. Reduction kinetics of Cu-, Ni-, and Fe-based oxygen carriers using syngas ($CO + H_2$) for chemical-looping combustion. Energy Fuels. 2007;21(4):1843–53.
18. Sahir AH, Lighty JS, Sohn HY. Kinetics of copper oxidation in the air reactor of a chemical looping combustion system using the law of additive reaction times. Ind Eng Chem Res. 2011;50(23):13330–9. doi:10.1021/ie2015779.
19. Sahir AH, Sohn HY, Leion H, Lighty JS. Rate analysis of chemical-looping with oxygen uncoupling (CLOU) for solid fuels. Energy Fuels. 2012;26(7):4395–404.
20. Eyring EM, Konya G, Lighty JS, Sahir AH, Sarofim AF, Whitty K. Chemical looping with copper oxide as carrier and coal as fuel. Oil Gas Sci Technol. 2011;66(2):209–21. doi:10.2516/Ogst/2010028.

21. Song H, Shah K, Doroodchi E, Wall T, Moghtaderi B. Analysis on chemical reaction kinetics of cuo/sio_2 oxygen carriers for chemical looping air separation. Energy Fuels. 2014;28(1):173–82.
22. Wang K, Yu QB, Qin Q. Reduction kinetics of Cu-Based oxygen carriers for chemical looping air separation. Energy Fuels. 2013;27(9):5466–74.
23. Wang K, Yu Q, Qin Q. The thermodynamic method for selecting oxygen carriers used for chemical looping air separation. J Therm Anal Calorim. 2013;112:747–53.
24. Clayton CK, Whitty KJ. Measurement and modeling of decomposition kinetics for copper oxide-based chemical looping with oxygen uncoupling. Appl Energy. 2014;116:416–23.
25. Adánez-Rubio I, Abad A, Gayan P, de Diego LF, Garcia-Labiano F, Adánez J. Identification of operational regions in the chemical-looping with oxygen uncoupling (CLOU) process with a Cu-based oxygen carrier. Fuel. 2012;102:634–45. doi:10.1016/j.fuel.2012.06.063.
26. Vyazovkin S, Burnham AK, Criado JM, Pérez-Maqueda LA, Popescu C, Sbirrazzuoli N. ICTAC Kinetics committee recommendations for performing kinetic computations on thermal analysis data. Thermochim Acta. 2011;520(1):1–19.
27. Starink M. A new method for the derivation of activation energies from experiments performed at constant heating rate. Thermochim Acta. 1996;288(1):97–104.
28. Šatava V. Mechanism and kinetics from non-isothermal TG traces. Thermochim Acta. 1971;2(5):423–8.
29. Doyle C. Kinetic analysis of thermogravimetric data. J Appl Polym Sci. 1961;5(15):285–92.
30. Brown ME, Dollimore D, Galwey AK. Reactions in the solid state. New York: Elsevier; 1980.
31. Zhang Y, Zhao H, Guo L, Zheng C. Decomposition mechanisms of Cu-based oxygen carriers for chemical looping with oxygen uncoupling based on density functional theory calculations. Combust Flame. 2015;162:1265–74.
32. Arjmand M, Keller M, Leion H, Mattisson T, Lyngfelt A. Oxygen release and oxidation rates of $MgAl_2O_4$-supported CuO oxygen carrier for chemical-looping combustion with oxygen uncoupling (CLOU). Energy Fuels. 2012;26(11):6528–39.
33. Kubaschewski O, Evans EL, Alcock C. Metallurgical thermochemistry. Oxford: Pergamon press; 1979.